Proceedings of the ASME 2021
International Design Engineering Technical Conferences and
Computers and Information in Engineering Conference
IDETC-CIE2021
August 17-19, 2021, Virtual, Online

DETC2021-71611

FEEDBACK CONTROL OF THE LOCOMOTION OF A TAILED QUADRUPED ROBOT

Yujiong Liu, Pinhas Ben-Tzvi*
Robotics and Mechatronics Laboratory
Mechanical Engineering Department
Virginia Tech
Blacksburg, VA, USA

ABSTRACT

The traditional locomotion paradigm of quadruped robots is to use dexterous (multi degrees of freedom) legs and dynamically optimized footholds to balance the body and achieve stable locomotion. With the introduction of a robotic tail, a new locomotion paradigm becomes possible as the balancing is achieved by the tail and the legs are only responsible for propulsion. Since the burden on the leg is reduced, leg complexity can be also reduced. This paper explores this new paradigm by tackling the dynamic locomotion control problem of a reduced complexity quadruped (RCQ) with a pendulum tail. For this specific control task, a new control strategy is proposed in a manner that the legs are planned to execute the open-loop gait motion in advance, while the tail is controlled in a closed-loop to prepare the quadruped body in the desired orientation. With these two parts working cooperatively, the quadruped achieves dynamic locomotion. Partial feedback linearization (PFL) controller is used for the closed-loop tail control. Pronking, bounding, and maneuvering are tested to evaluate the controller's performance. The results validate the proposed controller and demonstrate the feasibility and potential of the new locomotion paradigm.

1 INTRODUCTION

Locomotion using legs is usually thought to have better traversability compared to wheeled/tracked locomotion in unconstructed environments. At present, several quadruped robots have been successfully developed, including the well-known Big Dog series [1], HyQ [2], ANYmal [3], MIT Cheetah series [4], etc. The core locomotion technology behind these robots is the motion planning algorithm, which is to use optimization techniques to find the proper gait sequence, step-timing, footholds, as well as foot trajectory [5-7]. To simplify the control problem and maintain similar dexterity as quadrupedal animals, most quadrupedal robots chose a tailless structure with three degrees of freedom (DOF) legs.

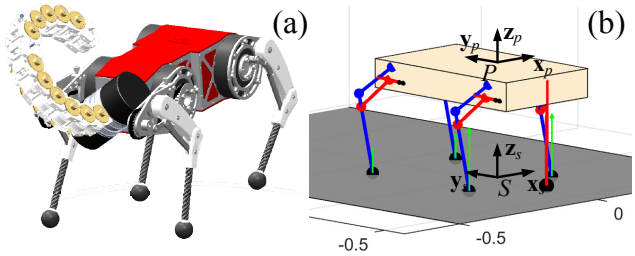

FIGURE 1. (a) The conceptual design of a reduced complexity quadruped (RCQ) with a biomimetic robotic tail realizing the new locomotion paradigm. (b) The abstract model used in this paper where the green arrows on the feet indicate the ground reaction force (GRF).

However, by looking to nature, tails are widely used as appendages for animals to assist in maneuvering, balancing, manipulation, and propelling. Among all these benefits, the core advantage is that the tail can provide a means of influencing the body dynamics independent of the leg's ground contact. Therefore, various case studies [8-14] were carried out to investigate the tail's usefulness in helping the locomotion of mobile robots. Although effective and successful, most existing research focuses on simple airborne righting tests and few trials on dynamic locomotion of legged robot have been conducted. As for the existing tail controllers, momentum-based tail motion planning and traditional trajectory tracking controller (e.g., PID) are the mainstream approaches. Nonlinear geometric control has not been applied yet, which has the potential advantage of being more stable and robust than the experience-based controllers.

Another important observation based on existing tail research is that after the tail was introduced to adjust the robot orientation, the mobile platform may no longer need a complicated leg system to achieve balance. The leg complexity (in terms of DOFs) could be reduced such that the legs are only

*Corresponding author – bentzvi@vt.edu

responsible for propelling. Following this idea, a new quadrupedal locomotion paradigm might be feasible whereby the leg complexity is reduced on the account of incorporating an onboard robotic tail system, especially multi-link tails since they can provide more control inputs. This newly proposed locomotion paradigm has several advantages, resulting in a simpler mechanical structure and fewer actuators due to the reduction of the DOFs in each leg. More importantly, with less control input from the leg, the focus of locomotion control is shifted from finding proper footholds to finding the proper tail controller, which is thought to be much simpler since the latter does not require direct interaction with the environment (the control problem degenerates into a classic nonlinear control problem) while the former usually leads to time-consuming, large scale, highly nonlinear optimization problem. However, this new paradigm also has trade-offs such that it does not have the same dexterous motion as the traditional quadruped. For instance, a traditional 12-DOF quadruped can change its orientation without moving its footholds while a simplified quadruped without abduction joints is unable to do this (unless using tail when the quadruped is airborne).

Therefore, this paper aims to explore this new paradigm by tackling the dynamic locomotion problem of a reduced complexity quadruped (RCQ) with a robotic tail, as shown in Fig. 1a. As the first step, the biomimetic tail is abstracted into a pendulum tail, and only pronking and bounding gaits are considered.

The contributions of this work are summarized as follows. (1) Dynamic locomotion of a point-feet reduced complexity quadruped with a pendulum tail, is achieved. (2) The results validate the feasibility and potential of the new locomotion paradigm, i.e. a simplified legged robot with a tail. (3) A new locomotion control framework that coordinates the open-loop leg motions and the closed-loop tail controller, is proposed. (4) Partial feedback linearization is successfully applied to formulate the tail controller.

The rest of this paper is organized as follows. Section 2 describes the robotic system and the dynamic modeling process. Section 3 presents the locomotion control framework that coordinates the leg motion and the tail motion. Section 4 applies the partial feedback linearization control technique to formulate the closed-loop tail controller. Section 5 describes the numerical experiments to verify the tail controller and to evaluate the locomotion performance.

2 ROBOT DESCRIPTION AND SYSTEM MODELING

This section presents relevant information about the target robotic system and the special modeling issues with the new system.

2.1 Single DOF Robotic Leg

The RCQ consists of four single DOF legs (previously proposed by the authors [15]) and one point-mass single-link tail. The leg mechanism and corresponding foot trajectory are shown in Fig. 2, where part i is the driving crank. Since the mechanism has only one DOF, the foot trajectory is a fixed curve and the only controllable variables are the crank position and the crank speed. The crank position has a one-to-one correspondence with a point on the foot trajectory and the associated pushing angle θ_p, which can largely determine how each leg pushes against the ground. The crank speed affects the pushing speed against the ground. These two variables together, determine the leg's ground pushing motion, which in turn generates the ground reaction force (GRF) that drives the quadruped motion. Therefore, the leg motion planning for the RCQ locomotion task requires determining the crank angle and the corresponding crank speed for the ground touchdown and liftoff events.

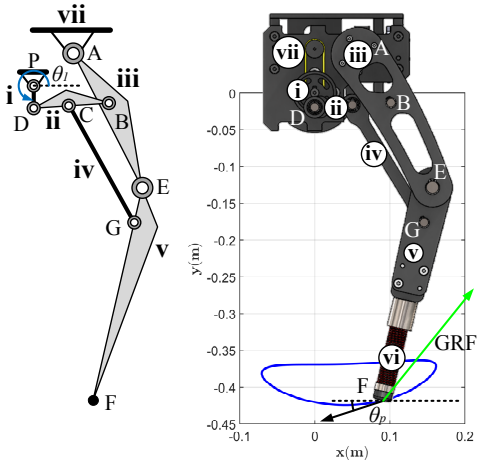

FIGURE 2. Left: kinematic diagram of the single DOF leg mechanism. Right: mechanical design of the single DOF robotic leg. Same label indicates the same link/joint.

2.2 Floating Base Dynamic Model

The traditional modeling process for multibody system dynamics usually requires defining a fixed body (usually the ground) as the root. This modeling approach demonstrated success in legged robot modeling, such as the point-foot biped [16] and the point-foot quadruped [17]. However, this is not the natural way that a body moves and the model number increases as the contact point increases (for instance, for a quadruped, there are 2^4=16 dynamic models). The transition among models increases even more as the model number increases. As a comparison, the floating-base model [18] frees the fixed connection between the ground and the robot, and uses environmental contact forces to drive the robot's motion. This modeling approach concurs more with the human's intuition and enables implementing properties of the environment (e.g., terrain information). This paper applies this modeling idea and the equation of motion (EOM) is formulated as

$$\mathbf{M}\ddot{\mathbf{q}} + \mathbf{H}(\mathbf{q}, \dot{\mathbf{q}}) = \mathbf{J}_{ta}^T \boldsymbol{\tau}_{ta} + \mathbf{J}_f^T \mathbf{f} \tag{1}$$

where $\mathbf{M} \in \mathbb{R}^{8\times8}$ is the system inertia matrix, and $\mathbf{H} \in \mathbb{R}^{8\times1}$ is the generalized loading due to Coriolis force, centrifugal force, and gravity. $\mathbf{J}_{ta} \in \mathbb{R}^{2\times8}$ and $\mathbf{J}_f \in \mathbb{R}^{12\times8}$ map the actuation

torque $\boldsymbol{\tau}_{ta} \in \mathbb{R}^{2\times1}$ and the GRF $\mathbf{f} \in \mathbb{R}^{12\times1}$ to the generalized space, respectively. Note that in this paper, only foot contacts are considered and the tail contacts with the ground as well as other body parts, are not considered. To reduce model complexity, the leg inertia is neglected in this paper based on the discussion in [7] that the swing leg motion usually has marginal influence on the quadruped's overall motion. This judgment is also the theoretical foundation of many well-known locomotion models, such as the linear inverted pendulum. However, neglecting the leg inertia only eliminates the appearance of the leg terms in the dynamic equations. The legs still participate in the locomotion task through ground pushing actions. Therefore, the generalized coordinates are chosen as $\mathbf{q} = [\mathbf{x}^T\ \boldsymbol{\phi}^T\ \boldsymbol{\alpha}^T]^T \in \mathbb{R}^3 \times \mathbb{S}^5$, where $\mathbf{x} \in \mathbb{R}^{3\times1}$ and $\boldsymbol{\phi} \in \mathbb{S}^{3\times1}$ are the quadruped torso position and orientation, respectively. $\boldsymbol{\alpha} \in \mathbb{S}^{2\times1}$ is the joint variables for the tail subsystem.

2.3 Equations of Motion Using Virtual Work Principle

The virtual work principle is used to find the components in Eq. (1). Referring to Fig. 1, the inertial frame $\Sigma S \coloneqq (S, \mathbf{x}_s, \mathbf{y}_s, \mathbf{z}_s)$ is attached to the ground and the body-fixed frame $\Sigma P \coloneqq (P, \mathbf{x}_p, \mathbf{y}_p, \mathbf{z}_p)$ is attached to the rectangle center P, which is formed by the four hip joint locations. The initial orientations of ΣP and ΣS are the same. The rotation matrix ${}^S\mathbf{R}_P$ from frame ΣP to ΣS is defined by the pitch (ϕ_x about $\mathbf{x}_s$), roll (ϕ_y about $\mathbf{y}_s$), and yaw (ϕ_z about $\mathbf{z}_s$) rotations with respect to the fixed axes. Therefore,

$$ {}^S\mathbf{R}_P = \mathbf{R}_z(\phi_z)\mathbf{R}_y(\phi_y)\mathbf{R}_x(\phi_x) \tag{2} $$

Then the torso angular velocity and angular acceleration are obtained as $\boldsymbol{\omega} = [\dot{\phi}_x\ \dot{\phi}_y\ \dot{\phi}_z]^T$ and $\dot{\boldsymbol{\omega}} = [\ddot{\phi}_x\ \ddot{\phi}_y\ \dot{\phi}_z]^T$, respectively. The tail variables $\boldsymbol{\alpha} = [\alpha_r\ \alpha_s]^T$ are defined with two consecutive relative rotations α_r and α_s about axis $\mathbf{y}_p$ and the rotated axis $\mathbf{x}_p$, respectively. The components in Eq. (1) are formulated as

$$ \mathbf{M} = m_b\mathbf{J}_{b,x}^T\mathbf{J}_{b,x} + \mathbf{J}_{b,\omega}^T\mathbf{I}_b\mathbf{J}_{b,\omega} + m_t\mathbf{J}_n^T\mathbf{J}_n \tag{3} $$

$$ \mathbf{H} = m_b\mathbf{J}_{b,x}^T\mathbf{g} + \mathbf{J}_{b,\omega}^T\tilde{\boldsymbol{\omega}}\mathbf{I}_b\boldsymbol{\omega} + m_t\mathbf{J}_n^T\mathbf{g} + m_t\mathbf{J}_n^T\dot{\mathbf{J}}_n\dot{\mathbf{q}} \tag{4} $$

$$ \mathbf{I}_b = {}^S\mathbf{R}_P\,{}^P\mathbf{I}_b\,{}^P\mathbf{R}_S \tag{5} $$

where $\mathbf{g} = [0\ 0\ g]^T$. m_b, m_t, and $\mathbf{I}_b$ are the torso mass, tail mass, and torso moment of inertia, respectively. $\mathbf{J}_{b,x}$, $\mathbf{J}_{b,\omega}$, and $\mathbf{J}_n$ are the Jacobians corresponding to the torso position $\mathbf{x}$, torso orientation $\boldsymbol{\phi}$, and tail tip displacement, respectively. All Jacobians including the foot displacement Jacobian $\mathbf{J}_f$ are computed manually.

2.4 Physics-based Contact Model

The classical approach to model the foot-ground contact is to assume that the ground is a rigid surface and the impact happens instantaneously [19]. However, this model misses important terrain information, and more importantly, it induces a sudden jump in the state space, which can lead to failure of the trajectory optimization (due to the resulting non-smooth Jacobian and Hessian matrices induced by the sudden jump). In comparison, the physical contact model [20] was proposed and used to model the foot-ground interaction. This paper applies this physics-based contact model and the GRF is computed as in Eq. (6) and the normal force $\mathbf{f}_n$ is modeled as a nonlinear spring-damper system.

$$ \mathbf{f} = \mathbf{f}_n + \mathbf{f}_f = \|\mathbf{f}_n\|\mathbf{z}_s + \|\mathbf{f}_x\|\mathbf{x}_s + \|\mathbf{f}_y\|\mathbf{y}_s \tag{6} $$

$$ \|\mathbf{f}_n\| = \max\{K_n z^{3/2} + D_n K_n z^{1/2}\dot{z},\ 0\} \tag{7} $$

The static friction is modeled as a linear spring-damper system while the kinetic friction is modeled using the classic Coulomb friction model. Therefore, the friction terms are calculated as

$$ \|\mathbf{f}_x\| = \begin{cases} \mu\|\mathbf{f}_n\|, & K_x x + D_x K_x \dot{x} > \mu\|\mathbf{f}_n\| \\ K_x x + D_x K_x \dot{x}, & \text{else} \\ -\mu\|\mathbf{f}_n\|, & K_x x + D_x K_x \dot{x} < -\mu\|\mathbf{f}_n\| \end{cases} \tag{8} $$

$\|\mathbf{f}_y\|$ takes the same form as $\|\mathbf{f}_x\|$, except replacing x with y.

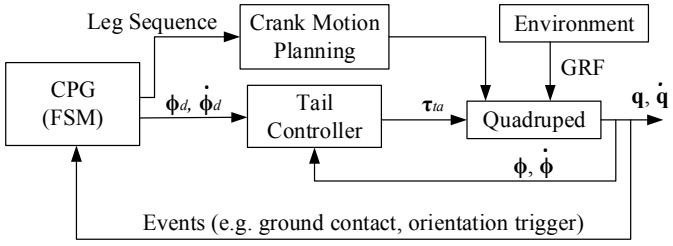

FIGURE 3. Locomotion controller structure for leg-tail coordination

3 EVENT-BASED LOCOMOTION CONTROL

Locomotion control considers the leg motion planning and the tail controller simultaneously. Namely, the leg and tail motions should work cooperatively to achieve the overall locomotion goal. This section addresses the coordination problem of the combined leg-tail system.

As shown in Fig. 3, the overall locomotion controller structure mainly consists of three modules: the central pattern generator (CPG), the tail controller, and the Crank Motion Planning (CMP) module. The CPG is essentially a finite state machine (FSM), which takes the events from the quadruped-environment interaction as inputs (for instance, front feet touch the ground or the body pitch angle reaches a certain value), triggers the state transition, and then executes the corresponding actions. The corresponding actions include determining the leg sequence, leg timing, tail controller switch (when to switch to which tail controller), and the tail controller objective $\boldsymbol{\phi}_d$.

The tail controller module contains two controller candidates. One is the tail orientation controller (TOC) which is used to adjust the quadruped orientation. The other is the resting damping controller (RDC) which is used to stabilize the tail motion. These two candidates are picked by the CPG depending on the actual FSM design. When the TOC is used, the CPG needs to determine the tail controller objective $\boldsymbol{\phi}_d$ which

defines the desired quadruped orientation (see Section 3.1 for more details).

The CMP module determines the crank motion parameters (e.g. start point, endpoint, rotation speed, and start time) for each leg based on the feed-in leg sequence information. Since the single DOF leg mechanism is optimized based on the assumption that the crank rotates at a constant speed, the CMP module also uses constant speed for each crank rotation. Note that due to the fixed foot trajectory, CMP can determine the crank motion directly by looking at the one-to-one correspondence table between the foot trajectory and the crank position. Since this paper neglects the leg inertia to simplify the analysis, the output of the CMP is directly fed into the quadruped to set the crank positions. For actual crank control with leg inertial loadings, another trajectory tracking module is required following the CMP module to generate the crank control torque. The following subsections detail the FSM design for specific locomotion modes.

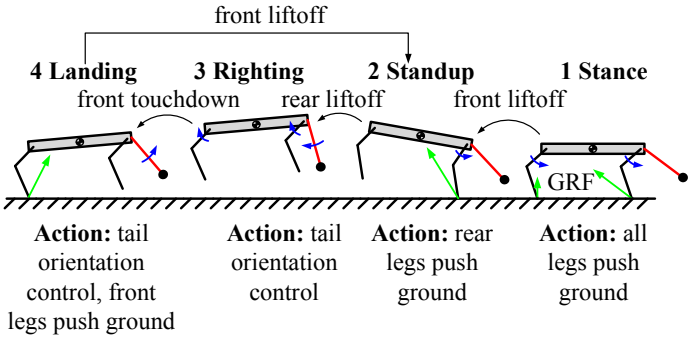

FIGURE 4. The bounding gait FSM design

3.1 Bounding Motion Planning

Bounding is the gait where the quadruped's front legs and rear legs touch the ground alternatively. For traditional quadruped robots with 3-DOF per leg, bounding is achieved by searching for the proper stance leg motion so that the torso orientation could be controlled indirectly. However, for the RCQ with a fixed feet curve, the foothold and the leg height cannot be controlled at the same time, which results in an uncontrollable torso orientation. Therefore, the tail system has to be used to achieve the bounding gait.

The FSM of the RCQ bounding gait is designed as shown in Fig. 4, where it mainly consists of three phases, including the standup phase, the righting phase, and the landing phase. The stance phase with four feet on the ground is the start point of the motion. The standup phase is triggered by the front legs lifting and ended by all feet leaving the ground. The righting phase refers to the airborne stage, and during this phase, the tail controller takes charge to adjust the torso orientation as needed. The landing phase follows the airborne righting phase and is triggered by only the front legs touching the ground. Note that the transition from the landing phase to the standup phase has to pass the stance phase. However, due to the short period of time (less than 0.1s) of this intermediate phase, the standup phase is connected with the landing phase directly inside the gait cycle. Based on the description in Section 2.1, the GRF is mainly determined by the leg configuration (crank position) and crank speed. However, it is also affected by the previous GRF and the overall loading distribution. For instance, due to the center of mass (COM) position and the extra weight from the tail, the rear feet usually have larger GRF than the front feet. Therefore, a larger crank speed is required for the rear legs to lift the whole quadruped. Moreover, to guarantee the proper functioning of the FSM, the cranks are set to go back to the same position ($\theta_1 = -50$ degrees) in every cycle before landing. This can avoid unpredictable GRFs and offers a subsequent standup phase similar to the initial condition. For the bounding gait, the RDC is not used during the locomotion cycle.

The core design parameters for the bounding motion planning are the crank speed, tail controller objective $\boldsymbol{\phi}_d$, and the timing to turn on the TOC. The crank speed is tuned manually by observing the bounding height. For a desired height of 0.6 meters, a crank speed of -25 rad/s is used. The tail controller objective is designed as $\boldsymbol{\phi}_d = [\phi_{xd}\ \phi_{yd}]^T = [-5\ \ 0]^T$ degrees for the righting phase and the TOC is turned on when $\phi_x > 10$ degrees. For the transition from the landing phase to the standup phase, $\boldsymbol{\phi}_d$ is set to $[5\ \ 0]^T$ degrees and the TOC keeps active as long as the feet are in contact with the ground.

3.2 Pronking Motion Planning

Pronking is a special case of bounding such that the standup landing phases are merged into the stance phase. To achieve this effect, the desired control objective is set to $\boldsymbol{\phi}_d = [\phi_{xd}\ \phi_{yd}]^T = [0\ \ 0]^T$ degrees. The TOC is turned on immediately after the feet leave the ground (flight phase). The same crank cycle position ($\theta_1 = -50$ degrees) and crank speed (-25 rad/s, which results in 0.55 meters high pronking) are used. The only difference from the bounding is that the RDC is used when the feet touch the ground.

3.3 Maneuvering

Using an active tail, maneuvering is thought easier in comparison with the traditional tailless quadruped because a tailed quadruped can just swing the tail to change its heading direction while a traditional quadruped needs to conduct a time-consuming trajectory optimization to find the proper maneuver motion. Therefore, to make the RCQ maneuver θ_m degrees, the $\boldsymbol{\phi}_d$ could be set as $[\phi_{xd}\ \phi_{yd}\ \phi_{zd}]^T = [0\ \ 0\ \ \theta_m]^T$ in the flight phase. However, since the control objectives (3 in this case) are more than the control inputs (the pendulum tail model used in this paper can only provide 2 inputs), the control objectives cannot be satisfied simultaneously, and the quadruped may experience unsmooth/unstable landing.

4 TAIL CONTROLLER FORMULATION

This section derives the tail controller mentioned in the previous section, based on the nonlinear feedback control formulation.

For the new locomotion paradigm, the core task of the tail system is to balance the quadruped during locomotion so that the simplified legs could focus on propelling. Therefore, a closed-loop tail controller that can automatically adjust the torso orientation is needed. Considering the high under-actuation characteristics of the system and the unnecessity of controlling tail position, the input-to-output partial feedback linearization (PFL) controller [21] is found suitable for this task. The "partial" here refers to the fact that this formulation only linearizes the selected state dynamics, in this case, the torso orientation $\boldsymbol{\phi}$.

Firstly, the desired output is constructed as

$$\mathbf{y} = \mathbf{q}_s - \mathbf{q}_d(t) \tag{9}$$

such that the selected states $\mathbf{q}_s = \mathbf{S}\mathbf{q}$ follows the desired trajectory $\mathbf{q}_d$ and $\mathbf{S} = \partial \mathbf{q}_s / \partial \mathbf{q}$ is the selection matrix, where s indicates the dimension of $\mathbf{q}_s$. Then the desired output dynamics could be constructed as

$$\ddot{\mathbf{y}} + \mathbf{K}_d \dot{\mathbf{y}} + \mathbf{K}_p \mathbf{y} = \mathbf{0} \tag{10}$$

where $\mathbf{K}_d = K_d \mathbf{I}_{s\times s}$ and $\mathbf{K}_p = K_p \mathbf{I}_{s\times s}$ with $K_d, K_p > 0$. Solving for $\ddot{\mathbf{q}}$ from Eq. (1) and extracting $\ddot{\mathbf{q}}_s$ from $\ddot{\mathbf{q}}$ yields

$$\ddot{\mathbf{q}}_s = \mathbf{S}\mathbf{M}^{-1}(\mathbf{J}_{ta}^T \boldsymbol{\tau}_{ta} - \mathbf{H}) \tag{11}$$

Substituting Eq. (11) into Eq. (10) and solving for $\boldsymbol{\tau}_{ta}$, the feedback controller is derived as

$$\boldsymbol{\tau}_{ta} = \mathbf{X}^+(\mathbf{S}\mathbf{M}^{-1}\mathbf{H} + \ddot{\mathbf{q}}_d + \mathbf{K}_d(\dot{\mathbf{q}}_d - \dot{\mathbf{q}}_s) + \mathbf{K}_p(\mathbf{q}_d - \mathbf{q}_s)) \tag{12}$$

in which $\mathbf{X} = \mathbf{S}\mathbf{M}^{-1}\mathbf{J}_{ta}^T$, and $\mathbf{X}^+$ indicates the Moore-Penrose inverse of $\mathbf{X}$.

The stability proof of the controller is straightforward. Substituting Eq. (12) back into the system dynamics yields

$$\mathbf{M}\ddot{\mathbf{q}} + \mathbf{H} = \mathbf{J}_{ta}^T \mathbf{X}^+(\mathbf{S}\mathbf{M}^{-1}\mathbf{H} + \ddot{\mathbf{q}}_d - \mathbf{K}_d\dot{\mathbf{y}} - \mathbf{K}_p\mathbf{y}) \tag{13}$$

Multiplying $\mathbf{X}^+\mathbf{S}\mathbf{M}^{-1}$ on both sides, Eq. (13) becomes

$$\mathbf{X}^+\ddot{\mathbf{q}}_s + \mathbf{X}^+\mathbf{S}\mathbf{M}^{-1}\mathbf{H} = \mathbf{X}^+\mathbf{X}\mathbf{X}^+(\mathbf{S}\mathbf{M}^{-1}\mathbf{H} + \ddot{\mathbf{q}}_d - \mathbf{K}_d\dot{\mathbf{y}} - \mathbf{K}_p\mathbf{y}) \tag{14}$$

which is further simplified to

$$\mathbf{X}^+(\ddot{\mathbf{y}} + \mathbf{K}_d\dot{\mathbf{y}} + \mathbf{K}_p\mathbf{y}) = \mathbf{0} \tag{15}$$

Therefore, if $s = 2$ (i.e. $\mathbf{X}$ is a square matrix), $\mathbf{X}^+ = \mathbf{X}^{-1}$ (assuming that $\mathbf{X}$ is away from its singularities). Then

$$\ddot{\mathbf{y}} + \mathbf{K}_d\dot{\mathbf{y}} + \mathbf{K}_p\mathbf{y} = \mathbf{0} \tag{16}$$

which is known to be exponentially stable (unforced damped harmonic oscillator). However, if $s \neq 2$ (i.e. $\mathbf{X}$ is not square), the stability may not be guaranteed. Specifically, if $s = 1$, $\mathbf{X}^+$ is column independent (2 by 1 matrix) such that the null space of Eq. (15) is the same as Eq. (16). The output $\mathbf{y}$ is still stable in this case. If $s > 2$, $\mathbf{X}^+$ is row independent such that the null space of Eq. (15) is no more than just a zero vector, which could expand to a line or a plane. In this case, the output stability is no longer guaranteed. Note that the controller is derived based on airborne dynamics ($\mathbf{f} = \mathbf{0}$). Stability is also not guaranteed after the feet are touching the ground. Moreover, in PFL, limitations on the tail range of motion are not applied.

4.1 Tail Orientation Controller (TOC)

When the quadruped is airborne, the control goal is to make sure that the robot lands on the ground at a desired orientation. Therefore, using the PFL formulation, the TOC is derived by setting the state error of the torso roll and pitch as the output function, i.e. $\mathbf{y} = [\phi_x - \phi_{xd} \;\; \phi_y - \phi_{yd}]^T$ where ϕ_{xd} and the ϕ_{yd} are the desired pitch and roll angles, respectively. As discussed before, $\mathbf{X}$ is invertible in this case and $\mathbf{X}^+ = \mathbf{X}^{-1}$. However, in some applications, the locomotion direction (yaw angle) may be also a control objective. For these cases, the output $\mathbf{y}$ could be chosen as $[\phi_x - \phi_{xd} \;\; \phi_y - \phi_{yd} \;\; \phi_z - \phi_{zd}]^T$ and the least square solution $\mathbf{X}^+ = (\mathbf{X}^T\mathbf{X})^{-1}\mathbf{X}^T$ maybe used to find the generalized inverse of $\mathbf{X}$. As for the one-dimensional output cases (e.g., the only motion of interest is rolling), $\mathbf{X}$ inverse is calculated as $\mathbf{X}^+ = \mathbf{X}^T(\mathbf{X}\mathbf{X}^T)^{-1}$.

4.2 Resting Damping Control (RDC)

When the quadruped is on the ground and is in a stable position, the active tail motion may not be necessary. For these situations, the tail controller should simply let the tail go back to its natural position. Therefore, the RDC is formulated as a simple pure damping system

$$\boldsymbol{\tau}_{ta} = -\,\mathrm{diag}([K_{d1} \;\; K_{d2}])\dot{\boldsymbol{\alpha}} \tag{17}$$

where $K_{d1}, K_{d2} > 0$ are the damping coefficients. Since this controller is equivalent to introducing friction into the tail joints, the system maintains its stability after switching to this controller. Note that this controller does not use the PFL formulation derived in the previous sections.

TABLE 1. RCQ parameters

Para.	Value	Para.	Value
m_b	12 Kg	K_n	5E4 Nm^{-1}
Torso Length	0.6 m	D_n	0.75
Torso Width	0.3 m	K_x, K_y	3E4 Nm^{-1}
Tail Length	0.45-0.9 m	D_x, D_y	0.01
${}^{p}\mathbf{I}_b$	diag([0.36 0.09 0.45]) Kgm^2	K_{d1}, K_{d2}	1
m_t	1 Kg	μ	1
g	9.8 ms^{-2}		

5 SIMULATION

All numerical computations were conducted in Matlab where the built-in function *ode45* with 1E-6 relative tolerance and 1E-8 absolute tolerance, was used for numerical integration. For the PFL controller output dynamics, the differentiation gain K_d is determined by setting the desired time constant to

$\tau = 0.02$ seconds so that the output could be zeroed in $5\tau = 0.1$ seconds (5τ guarantees 0.5% error). The proportional gain K_p was determined by the critical damping condition that reduces the oscillation. These two conditions yield

$$\tau = 2/K_d = 0.02 \Rightarrow K_d = 100 \quad (18)$$

$$K_d^2 - 4K_p = 0 \Rightarrow K_p = 2500 \quad (19)$$

All the RCQ parameters used are collected in Table 1, except for the leg dimensions which can be found in [15]. Tail torque saturation is set to 30Nm.

5.1 Pronking

Due to its simplicity, the first set of simulations is for the pronking gait where the quadruped is released in the air at a height of 0.5 meters and starts acting at 0.3 seconds. The simulation lasts 10 seconds and a longer tail (0.9 meters) is used to achieve more robust performance. Figure 5 shows the corresponding time response plots and the pitch angle ϕ_x phase portraits. From the figures, the pronking gait achieves stable locomotion and the phase portraits evolve in a bounded range.

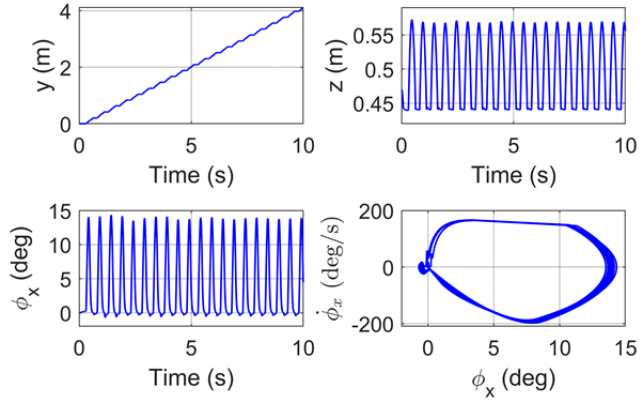

FIGURE 5. Pronking gait test: position information and phase portrait (bottom right)

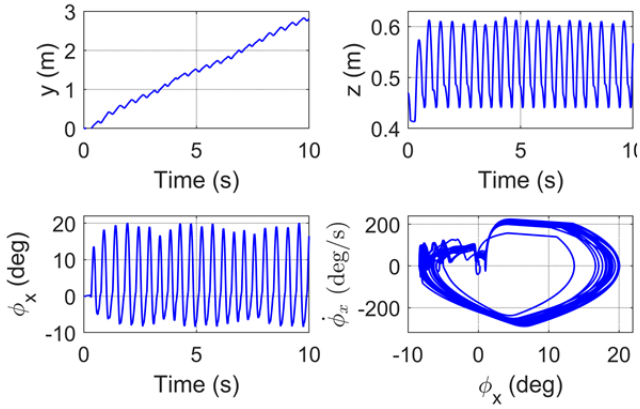

FIGURE 6. Bounding gait test: position information and phase portrait (bottom right)

5.2 Bounding

Using the same setup as the pronking gait, a bounding simulation is conducted. The time response plots and the pitch angle ϕ_x phase portraits are presented in Fig. 6. It can be found that due to the alternative foot contact, the bounding gait has two impact events (two nondifferentiable points in the z plot). The phase portrait is also more chaotic than the pronking gait. The GRF and the tail controller effort are also computed and presented in Fig. 7 where the "FL" and "FR" stand for the front left leg and the front right leg respectively. The "τ_r" and "τ_s" are the two components of $\boldsymbol{\tau}_{ta}$, in correspondence to the α_r joint and the α_s joint of the tail, respectively. From the figure, it can be found that the rolling joint is actually not used due to the fact that both the pronking and the bounding are essentially two gaits in the sagittal plane. It can be also found that the actual tail controller uses saturated torque for the orientation re-righting.

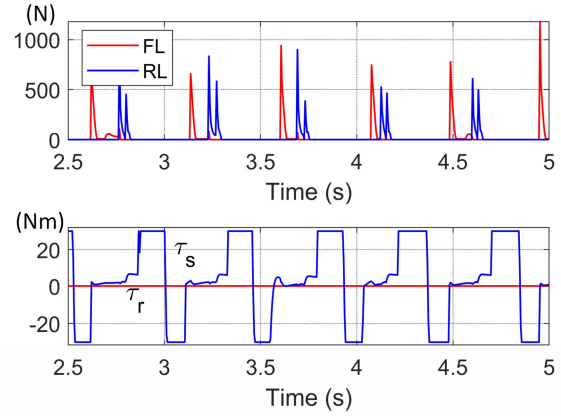

FIGURE 7. Bounding gait test: GRF and control effort

5.3 Maneuvering Case Study

As stated in Section 3.3, the two tail inputs are not able to fully control the three objectives in the maneuvering motion. Therefore, only a case study was performed, to observe the usefulness of the tail on the maneuvering locomotion. Figure 8 shows the snapshots of the maneuvering case study where a 0.45 meters long tail is used without applying torque saturation and θ_m is set to 15 degrees. Due to the least square solution (see Section 4.1), the tail controller cannot exactly track the desired control objective, which results in an actual turning angle of 16.45 degrees. This suggests that tails with more inputs should be used for fully controlling the quadruped orientation.

5.4 Discussion

It is worth noting that for the RCQ, due to the single DOF leg, if three legs touch the ground at the same time (equivalent to adding spherical joints between the feet and the ground), the mobility (the overall DOF) reduces to zero. Therefore, all gaits requiring three legs touching the ground at the same time (except for pronking since the spherical constraints introduced by pronking are redundant constraints) are impossible, e.g. walking and ambling. With help from the tail, all other gaits, namely, trotting, pacing, cantering, and galloping, are

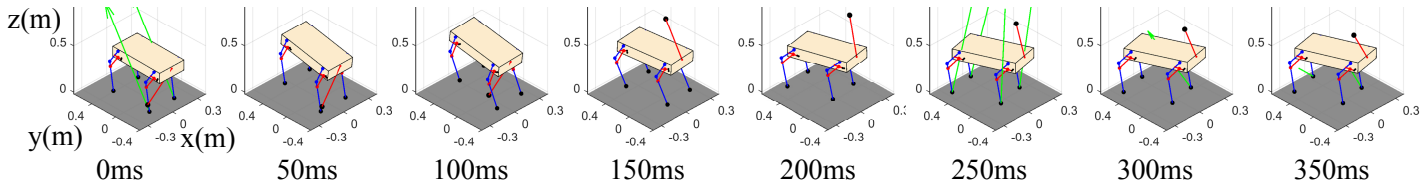

FIGURE 8. Snapshots for the maneuvering case study

theoretically possible.

In addition, one main deficiency observed for the current control strategy was that the tail motion range was not restricted, which is not possible in practice. Therefore, one focus for future work is to modify the tail controller such that the tail motion constraints could be introduced in the controller design stage, e.g. using numerical optimal control to impose state constraints in the PFL framework. However, for many applications such as the dynamics-based optimal design, the tail controller deficiency may not become a problem because these applications usually only consider the resultant whole robot performance, and the internal tail controller does not affect the overall performance due to the conservation of momentum.

6 CONCLUSION

This paper tackled the dynamic locomotion control problem of a point-feet reduced complexity quadruped that consists of four single DOF legs and one pendulum tail. Due to the special limitations on the legs, a tail is actively used to balance the quadruped while the legs are only responsible for propelling. To coordinate these two functions, a locomotion control framework that generates leg sequence, leg timing, and tail controller objective was proposed. The partial feedback linearization technique was used to formulate the closed-loop tail controller. Due to this special locomotion control strategy, no trajectory optimization was required. Three sets of numerical experiments including one pronking gait test, one bounding gait test, and one maneuvering case study, were conducted to verify the effectiveness of the tail controller and to evaluate the locomotion controller performance. The results validated the proposed control strategy.

ACKNOWLEDGMENTS

This material is partially based upon work supported by the National Science Foundation under Grant No. 1906727.

REFERENCES

[1] Raibert, M., Blankespoor, K., Nelson, G., and Playter, R., 2008, “Bigdog, the Rough-terrain Quadruped Robot,” IFAC Proceedings, 41(2), pp. 10822-10825.

[2] Semini, C., Tsagarakis, N.G., Guglielmino, E., Focchi, M., Cannella, F., and Caldwell, D.G., 2011, “Design of HyQ–a Hydraulically and Electrically Actuated Quadruped Robot,” Proceedings of the Institution of Mechanical Engineers, Part I: Journal of Systems and Control Engineering, 225(6), pp. 831-849.

[3] Hutter, M., Gehring, C., Jud, D., Lauber, A., Bellicoso, C.D., Tsounis, V., Hwangbo, J., Bodie, K., Fankhauser, P., Bloesch, M., and Diethelm, R., 2016, “Anymal-a Highly Mobile and Dynamic Quadrupedal Robot,” IEEE/RSJ International Conference on Intelligent Robots and Systems, Daejeon, South Korea, Oct. 9-14, 2016, pp. 38-44.

[4] Seok, S., Wang, A., Chuah, M.Y.M., Hyun, D.J., Lee, J., Otten, D.M., Lang, J.H., and Kim, S., 2014, “Design Principles for Energy-Efficient Legged Locomotion and Implementation on the MIT Cheetah Robot,” IEEE/ASME Transactions on Mechatronics, 20(3), pp. 1117-1129.

[5] Park, H.W., Wensing, P.M., and Kim, S., 2017, “High-speed Bounding with the MIT Cheetah 2: Control Design and Experiments,” The International Journal of Robotics Research, 36(2), pp. 167-192.

[6] Farshidian, F., Jelavic, E., Satapathy, A., Giftthaler, M., and Buchli, J., 2017, “Real-time Motion Planning of Legged Robots: A Model Predictive Control Approach,” IEEE-RAS 17th International Conference on Humanoid Robotics, Birmingham, UK, Nov. 15-17, 2017, pp. 577-584.

[7] Winkler, A.W., Bellicoso, C.D., Hutter, M., and Buchli, J., 2018, “Gait and Trajectory Optimization for Legged Systems Through Phase-based End-effector Parameterization,” IEEE Robotics and Automation Letters, 3(3), pp. 1560-1567.

[8] Patel, A., and Boje, E., 2015, "On the Conical Motion of a Two-degree-of-freedom Tail Inspired by the Cheetah," IEEE Transactions on Robotics, 31(6), pp. 1555-1560.

[9] Libby, T., Moore, T.Y., Chang-Siu, E., Li, D., Cohen, D.J., Jusufi, A., and Full, R.J., 2012, "Tail-assisted Pitch Control in Lizards, Robots and Dinosaurs," Nature, 481(7380), p. 181.

[10] Briggs, R., Lee, J., Haberland, M., and Kim, S., 2012, "Tails in Biomimetic Design: Analysis, Simulation, and Experiment," IEEE/RSJ International Conference on Intelligent Robots and Systems, Vilamoura, Portugal, Oct. 7-12, 2012, pp. 1473-1480.

[11] Chang-Siu, E., Libby, T., Brown, M., Full, R.J., and Tomizuka, M., 2013, “A Nonlinear Feedback Controller for Aerial Self-righting by a Tailed Robot,” IEEE International Conference on Robotics and Automation, Karlsruhe, Germany, May 6-10, 2013, pp. 32-39.

[12] Heim, S.W., Ajallooeian, M., Eckert, P., Vespignani, M., and Ijspeert, A.J., 2016, “On Designing an Active Tail for Legged Robots: Simplifying Control via Decoupling of

Control Objectives," Industrial Robot: An International Journal, 43(3), pp. 338-346.
[13] Rone, W.S., Liu, Y., and Ben-Tzvi, P., 2019, "Maneuvering and Stabilization Control of a Bipedal Robot with a Universal-spatial Robotic Tail," Bioinspiration & Biomimetics, 14(1), p. 016014.
[14] Saab, W., Yang, J., and Ben-Tzvi, P., 2018, "Modeling and Control of an Articulated Tail for Maneuvering a Reduced Degree of Freedom Legged Robot," IEEE/RSJ International Conference on Intelligent Robots and Systems, Madrid, Spain, Oct. 1–5, 2018, pp. 2695-2700.
[15] Liu, Y., and Ben-Tzvi, P., 2020, "An Articulated Closed Kinematic Chain Planar Robotic Leg for High Speed Locomotion," Journal of Mechanisms and Robotics, 12(4), p. 041003.
[16] Grizzle, J.W., Chevallereau, C., Sinnet, R.W., and Ames, A.D., 2014, "Models, Feedback Control, and Open Problems of 3D Bipedal Robotic Walking," Automatica, 50(8), pp. 1955-1988.
[17] Liu, Y., and Ben-Tzvi, P., 2021, "Dynamic Modeling, Analysis, and Comparative Study of a Quadruped with Bio-inspired Robotic Tails," Multibody System Dynamics, 51(2), pp. 195–219.
[18] Mistry, M., Buchli, J., and Schaal, S., 2010, "Inverse Dynamics Control of Floating Base Systems using Orthogonal Decomposition," IEEE International Conference on Robotics and Automation, Anchorage, AK, USA, May 3-7, 2010, pp. 3406-3412.
[19] Hurmuzlu, Y., GéNot, F., and Brogliato, B., 2004, "Modeling, Stability and Control of Biped Robots—a General Framework," Automatica, 40(10), pp. 1647-1664.
[20] Azad, M., and Featherstone, R., 2014, "A New Nonlinear Model of Contact Normal Force," IEEE Transactions on Robotics, 30(3), pp. 736-739.
[21] Spong, M.W., 1994, "Partial Feedback Linearization of Underactuated Mechanical Systems," IEEE/RSJ International Conference on Intelligent Robots and Systems, Munich, Germany, Sep. 12-16, 1994, pp. 314-321.